Modeling of cyclic hardening of metals coupled with martensitic transformation

Z. MRÓZ[1)], G. ZIĘTEK[2)]

[1)] *Institute of Fundamental Technological Research*
Warsaw, Poland

[2)] *Wroclaw University of Technology*
Wrocław, Poland

THE WORK PRESENTS an elasto-plastic material model with mixed hardening taking into account martensitic transformation. Modification of the kinematic hardening rule is proposed by relating back stress to the generalized thermodynamic force by a nonlinear function dependent on the fraction of martensite. The martensitic evolution is expressed in terms of isotropic hardening parameter by introducing proper free energy related force. The proposed model has been applied to predict hysteretic response for cyclic tension and compression tests for austenitic steel.

1. Introduction

MATERIAL UNDERGOING PHASE transformation, especially the martensite transition have been examined theoretically and experimentally for more than 50 years. Such phase transformation may occur in certain types of austenitic steels, so-called metastable ones, such as high manganium or high nickel steels. This transformation takes place as a result of varying temperature, applied stress or by induced plastic strain. The transformation caused by stress or plastic strain, so called athermal transformation, takes place even at room temperature (also induced by cyclic loading). The ample literature in the area of athermal transformation is devoted to the effect commonly known as TRIP (transformation induced plasticity).

The present paper provides the discussion of another problem, namely the martensitic transformation induced by plastic strain (PIMT). Such transformation can substantially affect mechanical properties by increasing the hardening rate and the form of hysteresis loops, generated in the cyclic loading process. Figure 1 presents the steady cyclic loops obtained for AS 304L steel at different strain amplitudes by KALETA and ZIĘTEK, [1]. The majority of papers, especially the experimental ones devoted to this problem, examine mostly monotonic loading (LEBEDEV *et al.* [2], GANESH *et al.* [3], PIWECKI, [4]). However such transformation occurs also under cyclic loading (MUGHRABI *et al.* [5],

Sugimoto *et al.* [6], Kaleta   *et al.* [1], Garion *et al.* [7]), and it can substantially affect material properties. Only microscopic observations and structural examinations performed, for example, by means of electron microscope can determine the amount of existing martensite. The paper of Kaleta and Ziętek [1], presents results of such examinations indicating appearance of the α' martensite inside austenite under uniaxial cyclic strain. It is seen that the hardening modulus increases starting from some value of plastic strain in both compressive and tensile semi-cycles. There is a characteristic inflection point on the cyclic skeletal curve connecting the tips of hysteresis loops, Fig. 1.
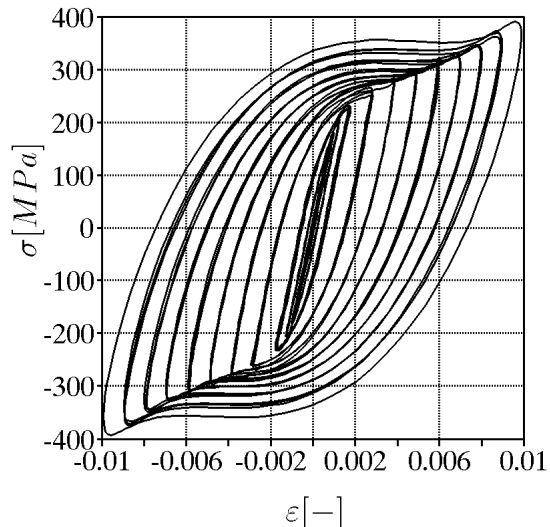

Fig. 1. Cyclic stress-strain curve and steady state $\sigma - \varepsilon$ loops for strain controlled cyclic loading (from Kaleta and Ziętek, [1]).

Phenomenological constitutive equations are usually formulated within the framework of irreversible thermodynamics with account for internal state variables ([8]). This allows for the analysis of kinetics of deformation processes as well as of evolution of generalized thermodynamic forces. The two-phase material is then treated as a thermodynamical system with two irreversible processes, namely, phase transformation and plastic deformation. The selection of internal variables and macroscopic parameters is essential for this approach. The volume fraction of martensite ξ is the most popular macroscopic internal variable specifying the growth of martensitic phase [9, 10]. The derived evolution equation for this parameter together with suitable model of material hardening provides a complete set of equations specifying the response, with account for structural changes induced by martensitic transformation. In Sec. 2 we propose a simple constitutive model of plastic response with the combined isotropic-kinematic

hardening and cyclic stress evolution dependent on martensite volume fraction ξ. The specification of material functions and parameters is presented in Sec. 3. The model is applied to simulate cyclic response of steel with some examples presented in Sec. 4.

2. Elastic-plastic model

To formulate the constitutive relations, assume the combined (isotropic-kinematic) hardening model. A familiar Huber–Mises yield condition takes the form

$$(2.1) \qquad F_p = \sqrt{\frac{3}{2}(s_{ij} - f_{ij})(s_{ij} - f_{ij})} - R(\kappa) \leq 0,$$

where s_{ij} is the stress deviator, $R(\kappa)$ denotes the yield surface radius (size) and κ is the monotonically increasing accumulated plastic strain measure. The yield surface centre is specified by the deviatoric tensor f_{ij} related to the back stress X_{ij} by the following equation:

$$(2.2) \quad f_{ij} = X_{ij}(1 + aX_{mn}X_{mn}), \qquad \text{or} \quad \mathbf{f} = \mathbf{X}(1 + a\mathbf{X} \cdot \mathbf{X}) = \mathbf{X}(1 + aX^2),$$

where $X^2 = \mathbf{X}{\cdot}\mathbf{X}$ and $a = a(\xi) > 0$ is the function of the martensite volume fraction, so that $a(0) = 0$. Thus, for $\xi = 0$, we obtain the classical kinematic hardening model with the back stress $\mathbf{X} = [X_{ij}]$ representing the yield surface centre. The dot between two vector or tensor symbols denotes their scalar product.

The back stress X_{ij} does not correspond to the yield surface centre for $a > 0$ (Fig. 2). It is shifted by the vector

$$(2.3) \qquad f_{ij} - X_{ij} = (aX_{kl}X_{kl})X_{ij},$$

which depends on the martensite volume fraction and is proportional to the second invariant of the back stress.

The yield surface specifies the regimes of plastic flow and elastic deformation. Additionally, we have to formulate the condition of martensite transformation in the form

$$(2.4) \qquad F_{tr} = \Sigma - G(\xi, \kappa) \leq 0,$$

where Σ denotes the generalized transformation force conjugate with ξ and $G(\xi, \kappa)$ is the dissipative force dependent on both plastic strain and martensite volume fraction, thus allowing for the analysis of coupled effect of two irreversible processes.
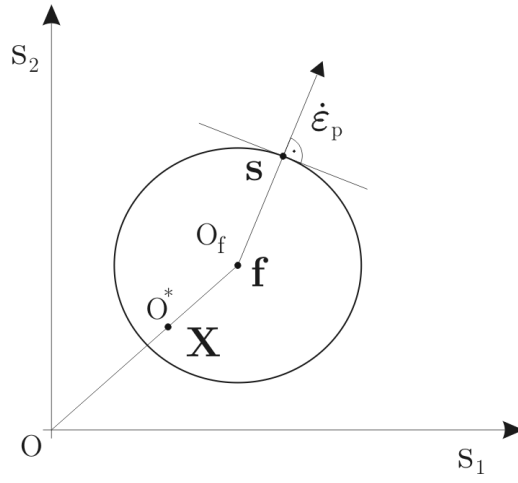
Fig. 2. The yield surface with back stress shifted from the surface centre.

The elastic state of material can be specified in terms of state variables $\boldsymbol{\alpha}_1$ and conjugate forces $\mathbf{A}_1$,

$$(2.5) \qquad \boldsymbol{\alpha}_1 = (\boldsymbol{\varepsilon}^{\mathbf{e}}, T) \rightarrow \mathbf{A}_1 = (\boldsymbol{\sigma}, S)$$

where $\boldsymbol{\varepsilon}^{\mathbf{e}} = \left[\varepsilon_{ij}^e \right]$ is the elastic strain tensor, T denotes the temperature, $\boldsymbol{\sigma} = [\sigma_{ij}]$ is the Cauchy stress tensor and S is the specific entropy per unit mass. The hardening state is specified in terms of internal state variables and conjugate generalized forces

$$(2.6) \qquad \boldsymbol{\alpha}_2 = (\boldsymbol{\eta}, \xi, \kappa) \rightarrow \mathbf{A}_2 = (\mathbf{X}, \varSigma, R)$$

where $\boldsymbol{\eta} = [\eta_{ij}]$ is the microstrain conjugate to the back stress $\mathbf{X}$.

The specific free energy $\tilde{\varPsi}$ per unit mass is assumed to be a function of state and internal variables. For an isothermal process, assume the following form as a sum of elastic and stored energies:

$$(2.7) \qquad \rho\tilde{\varPsi} = \varPsi(\boldsymbol{\alpha}_1, \boldsymbol{\alpha}_2) = \frac{1}{2} \varLambda_{ijkl} \varepsilon_{ij}^e \varepsilon_{kl}^e + \frac{1}{2} C_1 \eta_{ij} \eta_{ij} + \varphi(\xi, \kappa)$$

where ρ is the mass density. The conjugate forces are specified from the potential relations, thus

$$(2.8) \qquad
\begin{aligned}
\sigma_{ij} &= \frac{\partial \varPsi}{\partial \varepsilon_{ij}^e} = \varLambda_{ijkl} \varepsilon_{kl}^e, & X_{ij} &= \frac{\partial \varPsi}{\partial \eta_{ij}} = C_1 \eta_{ij}, \\
\varSigma &= \frac{\partial \varPsi}{\partial \xi} = \frac{\partial \varphi}{\partial \xi}, & R &= \frac{\partial \varPsi}{\partial \kappa} = \frac{\partial \varphi}{\partial \kappa},
\end{aligned}$$

where $\varLambda_{ijkl}$ is the tensor of elastic stiffness moduli.

Assume the total strain as a sum of elastic and inelastic components, thus

$$(2.9) \qquad \varepsilon_{ij} = \varepsilon_{ij}^e + \varepsilon_{ij}^p$$

where

$$(2.10) \qquad \varepsilon_{ij}^p = \varepsilon_{ij}^s + \varepsilon_{ij}^{tr}.$$

Here ε_{ij}^s denotes the plastic strain due to polycrystalline slip and ε_{ij}^{tr} is the transformation strain induced by martensite combined with twinning. In our model formulation, we shall not make distinction between ε_{ij}^s and ε_{ij}^{tr} as it is difficult to specify this irreversible strain decomposition experimentally.

For the increasing stress, we have first the case of plastic deformation, so that

$$(2.11) \qquad F_p = 0, \qquad \dot{F}_p = 0 \quad \text{and} \quad F_{tr} < 0$$

and no martensite transformation occurs. The associated flow rule specifies the plastic strain rate and the non-associated evolution rules specify the microstrain and the back stress rate, thus

$$(2.12) \qquad \dot{\varepsilon}_{ij}^p = \dot{\lambda}_1 \frac{\partial F_p}{\partial \sigma_{ij}} = \dot{\lambda}_1 \frac{3(s_{ij} - f_{ij})}{2R},$$

$$(2.13) \qquad \dot{\eta}_{ij} = -\dot{\lambda}_1 \left(\frac{\partial F_p}{\partial X_{ij}} + \frac{\partial \Psi^r}{\partial X_{ij}} \right), \qquad \Psi^r = \frac{1}{2} C X_{ij} X_{ij}$$

and

$$(2.14) \qquad \dot{\kappa} = -\dot{\lambda}_1 \frac{\partial F_p}{\partial R} = \dot{\lambda}_1.$$

In writing (2.13), we introduce the recovery potential $\Psi^r = \Psi^r(X_{ij})$ by assuming the evolution of back stress to be governed by the hardening and recovery processes. In view of (2.8), we have

$$(2.15) \qquad \dot{X}_{ij} = C_1 \dot{\eta}_{ij} = C_1 A_{ijkl} \dot{\varepsilon}_{kl}^p - \dot{\lambda}_1 C_1 C X_{ij}$$

where

$$(2.16) \qquad A_{ijkl} = \delta_{ijkl}[1 + aX_{mn}X_{mn}] + 2aX_{ij}X_{kl}$$

and δ_{ijkl} is the unit tensor. Let us note that for $a = 0$, the back stress evolution rule (2.15) becomes the familiar Frederick–Armstrong rule

$$(2.17) \qquad \dot{X}_{ij} = C_1 \dot{\varepsilon}_{ij}^p - \dot{\lambda}_1 C_1 C X_{ij}$$

accounting in a simple way for hardening and recovery effects. It is clear that for constant values of C_1 and C, the back stress evolves to the limit surface $\overline{F}_l(\mathbf{X}) = 0$. In fact, setting $\dot{X}_{ij} = 0$ at the limit state, from (2.17) we obtain

$$(2.18) \qquad\qquad X_{ij} = \frac{1}{C}\frac{3(s_{ij} - X_{ij})}{2R}$$

and in view of (2.1) there is a limit surface in the back stress space specified by

$$(2.19) \qquad \overline{F}_l(\mathbf{X}) = \sqrt{\frac{3}{2}X_{ij}X_{ij}} - R_x = 0, \qquad R_x = \frac{3}{2C}.$$

Similarly, in the stress space we have

$$(2.20) \qquad F_l(\boldsymbol{\sigma}) = \sqrt{\frac{3}{2}s_{ij}s_{ij}} - R_l = 0, \qquad R_l = R + \frac{3}{2C}.$$

Equations (2.19) and (2.20) specify the limit surface in respective spaces. The transformation rule (2.17) can now be rewritten in the form

$$(2.21) \qquad\qquad \dot{\mathbf{X}} = \dot{\lambda}_1(\mathbf{s}_l - \mathbf{s})\gamma = \dot{\lambda}_1(\mathbf{X}_l - \mathbf{X})CC_1$$

where $\mathbf{s}_l$ and $\mathbf{X}_l$ are the limit states on the surfaces $F_l(\boldsymbol{\sigma})$ and $F_l(\mathbf{X})$ corresponding to the same normal vector of the yield surface at the current state, Fig. 3, thus

$$(2.22) \qquad \mathbf{s}_l = (\mathbf{s} - \mathbf{X})\left(1 + \frac{3}{2RC}\right), \qquad \mathbf{X}_l = \frac{3}{2RC}(\mathbf{s} - \mathbf{X}).$$

Figure 3a illustrates the evolution rule (2.21). The back stress evolves along the vector $(\mathbf{s}_l - \mathbf{s})$ or $(\mathbf{X}_l - \mathbf{X})$ tending to the limit state $\mathbf{X}_l$ for constant orientation
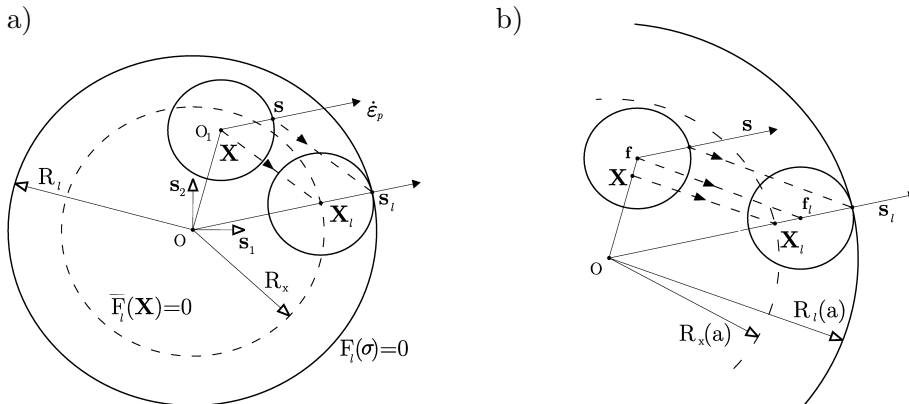

FIG. 3. Evolution of the back stress $\mathbf{X}$ to the limit state $\mathbf{X}_l$, specified by a) Eq. (2.21) and b) Eq. (2.15).

of the plastic strain rate vector. Let us note that the *coaxiality rule* occurs at the limit state between $\mathbf{X}_l$ and $\dot{\boldsymbol{\varepsilon}}^p$. Let us note that evolution rule (2.21) is identical to that proposed by MRÓZ [11], in formulating the multisurface hardening model, and next extended by MRÓZ and RODZIK [12], in order to simulate quantitatively ratcheting and memory effects in cyclic deformation.

Consider now the evolution rule (2.15) which can be rewritten in the form

$$(2.23) \quad \dot{X}_{ij} = C_1 \dot{\lambda}_1 \left[\frac{3(s_{ij} - f_{ij})}{2R}(1 + aX^2) + 3a\frac{X_{kl}(s_{kl} - f_{kl})}{R}X_{ij} - CX_{ij} \right].$$

If a limit state exists, then $\dot{X}_{ij} = 0$, and

$$(2.24) \qquad \left[\frac{3(s_{ij} - f_{ij})}{2R}(1 + aX^2) + 3a\frac{X_{kl}(s_{kl} - f_{kl})}{R}X_{ij} \right] - CX_{ij} = 0$$

so the coaxiality rule occurs, namely

$$(2.25) \qquad \frac{1}{1 + aX^2}\left(C - 3a\frac{\mathbf{X} \cdot (\mathbf{s} - \mathbf{f})}{R} \right)\mathbf{X} = \frac{3(\mathbf{s} - \mathbf{f})}{2R}$$

and the transition rule (2.21) remains valid, see Fig. 3b.

Equations (2.24) multiplied by $\dfrac{3(s_{ij} - f_{ij})}{2R}$ and X_{ij} provide the system of two scalar equations

$$(2.26) \qquad \left[\frac{3}{2}(1 + aX^2) + 2a\left(\frac{3\mathbf{X} \cdot (\mathbf{s} - \mathbf{f})}{2R} \right)^2 \right] - C\frac{3\mathbf{X} \cdot (\mathbf{s} - \mathbf{f})}{2R} = 0,$$

$$\left[(1 + aX^2)\frac{3\mathbf{X} \cdot (\mathbf{s} - \mathbf{f})}{2R} + 2a\left(\frac{3\mathbf{X} \cdot (\mathbf{s} - \mathbf{f})}{2R} \right)X^2 \right] - CX^2 = 0,$$

with two unknowns, X^2 and $\dfrac{3\mathbf{X} \cdot (\mathbf{s} - \mathbf{f})}{2R}$. After rearrangements, we arrive at the equation specifying the size of the limit surface in the form

$$(2.27) \qquad \left(aX^2 + 1 \right)\left(X^2 - \frac{C^2 - 9a - C\sqrt{C^2 - 18a}}{27a^2} \right)$$

$$\cdot \left(X^2 - \frac{C^2 - 9a + C\sqrt{C^2 - 18a}}{27a^2} \right) = 0.$$

Equation (2.27) has no positive roots when

$$(2.28) \qquad\qquad\qquad 18a \geq C^2$$

and then the limit surface does not exist. Thus when $a = 0$, $\xi = 0$ at the initial transformation state, the evolution rule (2.17) or (2.21) predicts the usual saturation value of the back stress. Assuming the monotonic function $a = a(\xi)$, the critical value $a_c = a(\xi_c) = C^2/18$ is reached and for $a > a_c$ the limit surface does not exist. The hardening process is strongly affected by the increasing martensite fraction and for $\xi > \xi_c$ it dominates over the recovery process.

The hardening modulus H can be determined from the consistency condition

$$(2.29) \qquad \frac{\partial F_p}{\partial \sigma_{ij}} \dot{\sigma}_{ij} - \dot{\lambda}_1 H = 0,$$

and we obtain

$$(2.30) \qquad H = \{A_{ijkl}\} \frac{\partial F_p}{\partial \sigma_{kl}} \left(C_1 \{A_{ijmn}\} \frac{\partial F_p}{\partial \sigma_{mn}} - \gamma X_{ij} \right) + \frac{\partial R}{\partial \kappa}$$

$$= \frac{3}{2} \left\{ C_1 (1 + aX^2)^2 + 6aC_1 \left(\frac{\mathbf{X} \cdot (\mathbf{s} - \mathbf{f})}{R} \right)^2 (1 + aX^2) \right.$$

$$\left. + \frac{\mathbf{X} \cdot (\mathbf{s} - \mathbf{f})}{R} \left(X^2 C_1 (4a^2 - 2aC - \frac{3}{2}C) \right) \right\} + \frac{\partial R}{\partial \kappa}.$$

The parameter κ is proportional to the length of the plastic strain trajectory. The martensitic transformation process proceeds when κ reaches the critical value κ_c, and then we have

$$(2.31) \qquad F_p = 0, \qquad \dot{F}_p = 0 \qquad \text{and} \qquad F_{tr} = 0, \qquad \dot{F}_{tr} = 0.$$

The evolution rule for the volume fraction of martensite has a form

$$(2.32) \qquad \dot{\xi} = -\dot{\lambda}_2 \frac{\partial F_{tr}}{\partial \Sigma} = -\dot{\lambda}_2.$$

In view of Eq. (2.4), we have

$$(2.33) \qquad \dot{\lambda}_2 = \frac{\Sigma_\kappa - G_\kappa}{G_\xi - \Sigma_\xi} \dot{\kappa}$$

where

$$(2.34) \qquad G_\kappa = \frac{\partial G}{\partial \kappa}, \qquad G_\xi = \frac{\partial G}{\partial \xi}, \qquad \Sigma_\kappa = \frac{\partial \Sigma}{\partial \kappa}, \qquad \Sigma_\xi = \frac{\partial \Sigma}{\partial \xi}.$$

3. Selection of free energy function and material parameters

Appropriate forms of the functions $\varphi(\xi, \kappa)$ and $G(\xi, \kappa)$ must be selected in order to describe the coupled process of the martensitic transformation and the plastic deformation. Assume the condition that both, the yield surface radius R and the martensite volume fraction ξ tend to limit values R^* and ξ^* for increasing accumulated plastic strain, $\kappa \to \infty$. Assume that the stored free energy function is of the form

$$(3.1) \qquad \varphi(\xi, \kappa) = a_1\xi\kappa + a_2\kappa + a_3\left(e^{-a_4\kappa} - 1\right),$$

where $0 \leq \xi \leq 1$ and $\kappa \geq 0$. The first term of (3.1) represents the stored free energy associated with martensite transformation and the effective accumulated plastic strain and the subsequent terms provide the variation of the radius R due to plastic hardening, so that

$$R = a_1\xi + a_2 - a_3a_4e^{-a_4\kappa},$$

$$(3.2)$$

$$\Sigma = \frac{\partial\varphi}{\partial\xi} = a_1\kappa.$$

Assuming the form of the function $G(\xi, \kappa)$, we may obtain the relation between the parameter ξ and the effective accumulated plastic strain

$$(3.3) \qquad G(\xi, \kappa) = \frac{b_1\xi\kappa}{b_2 - e^{-b_3\kappa}} + G_o.$$

Taking into account Eqs. (2.4), (3.2) and (3.3), we have the martensite evolution rule in the form

$$\xi = \xi^*\left(1 - \frac{\kappa_c}{\kappa}\right)\left(1 - \frac{1}{b_2}e^{-b_3\kappa}\right), \qquad \xi^* = \frac{a_1b_2}{b_1}$$

$$(3.4)$$

$$\text{and} \qquad \kappa \geq \kappa_c = \frac{G_o}{a_1}.$$

The martensite volume fraction ξ and the yield surface radius converge asymptotically to limit values

$$(3.5) \qquad \xi \xrightarrow[\kappa\to\infty]{} \xi^* \qquad \text{and} \qquad R \xrightarrow[\kappa\to\infty]{} a_1\xi^* + a_2.$$

The parameter a occurring in Eq. (2.3) is the function of the martensite volume fraction ξ, so it converges to a limit value a^*

$$(3.6) \qquad a\left[\xi\left(\kappa\right)\right] \xrightarrow[\kappa\to\infty]{} a^* = a(\xi^*).$$

a)

b)
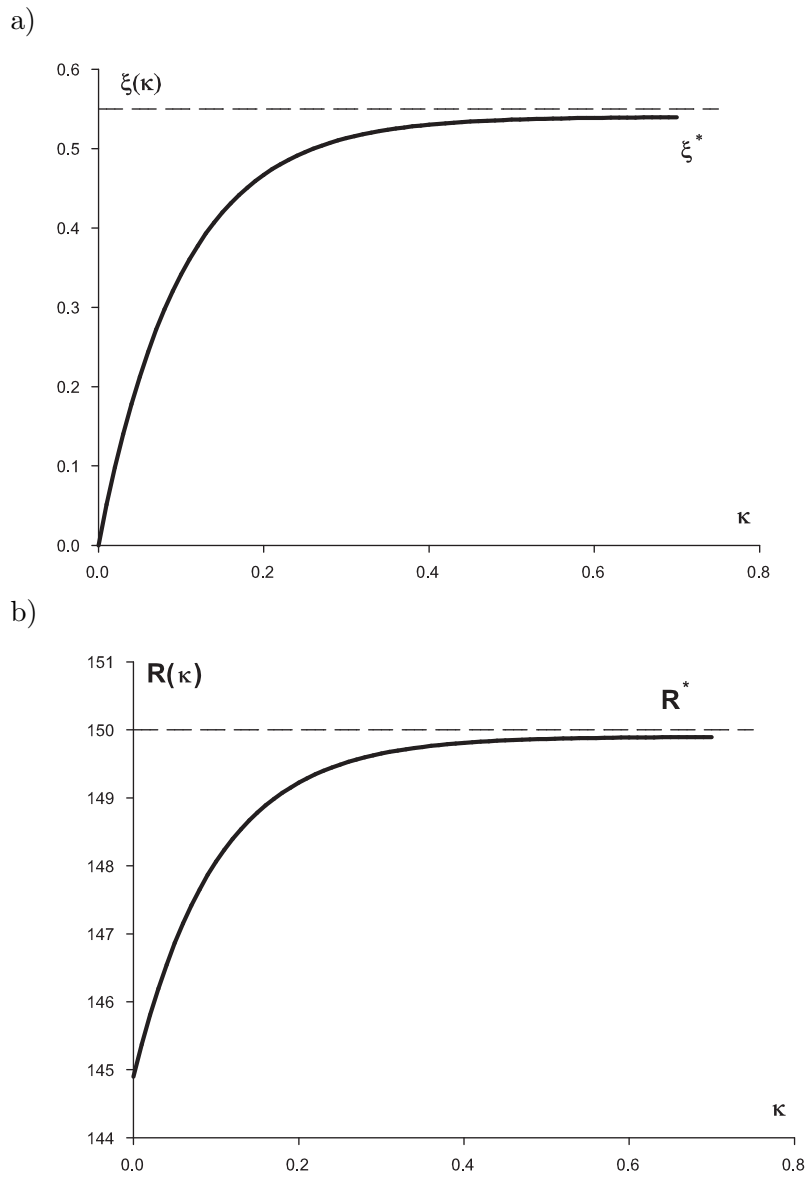

FIG. 4. The form of functions a) $\xi = \xi(\kappa)$, b) $R = R(\kappa)$.

4. Application of constitutive model: evolution of hysteresis loops in uniaxial cyclic straining

The model identification was performed for the exemplary martensitic transformation in steel AISI 304L. The deformation process of cylindrical specimens

was examined in the cyclic uniaxial tension – compression tests. The control was imposed on the amplitude of the plastic strain ε_{ap}. The measured quantities are total strain ε, elastic strain ε_e and the stress σ in the cyclic deformation process. The details of performed experiments and their results are presented in [1]. Approximation has been performed making use of the package PLOT 4.0.

For the uniaxial tension-compression, Eqs. (2.1) and (2.15) take the form

$$(4.1) \qquad \left| \sigma - X - a(\xi)X^3 \right| = R,$$

$$(4.2) \qquad \dot{X} = \frac{3}{2}C_1(1 + 2a(\xi)X^2)\dot{\varepsilon}_p - C_1CX\,|\dot{\varepsilon}_p|$$

where $|\dot{\varepsilon}_p| = \dot{\lambda}_1$. Denoting by $\dot{X}$ the derivative $dX/d\lambda_1$ from (4.2) we obtain two equations specifying the evolution of X for tension and compression events, namely

$$(4.3) \qquad \begin{aligned} \dot{X}^t &= \frac{3}{2}C_1 - \gamma X + 3C_1^a(\xi)X^2, & \dot{\varepsilon}_p &> 0, \\[2mm] \dot{X}^c &= \frac{3}{2}C_1 + \gamma X + 3C_1^a(\xi)X^2, & \dot{\varepsilon}_p &< 0 \end{aligned}$$

where $\gamma = CC_1$.

Figure 5a presents the variation of $\dot{X}$ following the rules (4.3). It is seen that for $X = \pm C/6a$ (points K and L in Fig. 5a) the rate of back stress increases on both the tension and compression paths. The stress-strain hysteresis loop then exhibits inflection points with increased rate of hardening (points K'' and L' in Fig. 5b). To preserve the positive values of $\dot{X}^t$ and $\dot{X}^c$, the discriminant of the quadratic forms (4.3) should be negative definite so that $a(\xi_c) > C^2/18$. This inequality is identical to (2.28) derived for the general stress state.

When $a(\xi) \leq a(\xi_c)$, then the limit surface exists and recovery process dominates over the hardening process, thus assuring the saturation state. There are two real roots for the parabolas (4.3). The root

$$(4.4) \qquad X_{\lim} = \frac{C - \sqrt{C^2 - 18a}}{6a}$$

determines the limit value of the back stress. $X_{\lim} \xrightarrow[a \to 0]{} \dfrac{3}{2C}$ and $X_{\lim}\,(a(\xi_c)) = \dfrac{3}{C}$, so $\dfrac{3}{2C} \leq X_{\lim} \leq \dfrac{3}{C}$. Figure 6 presents the variation of $\dot{X}$ and the corresponding back stress – strain hysteresis loop.
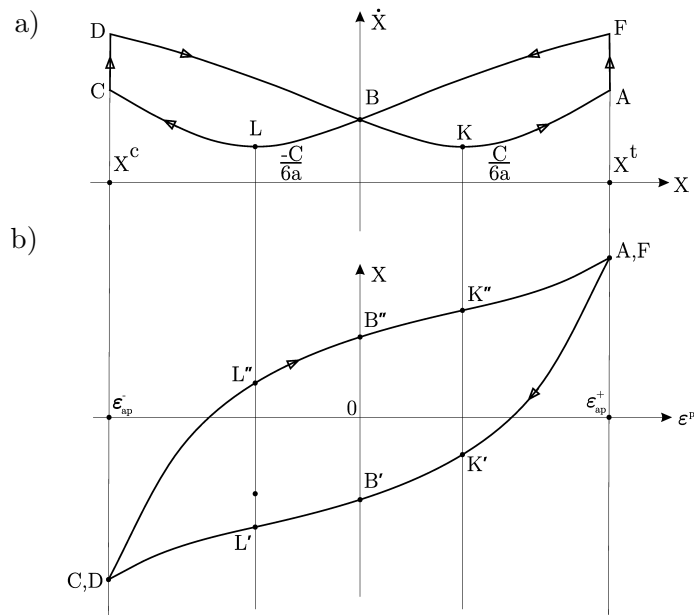
FIG. 5. Back stress evolution for $a(\xi) > a(\xi_c)$ in cyclic deformation: a) variation of the rate of back stress, b) back stress hysteresis loop.
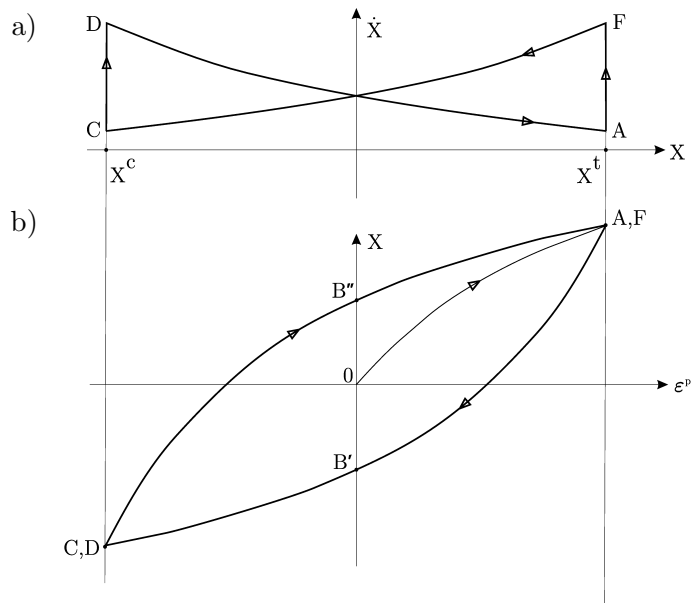

FIG. 6. Back stress evolution for the case $a(\xi) \leq a(\xi_c)$: a) variation of rate of back stress, b) back stress hysteresis loop.

Now there is no inflection point on the X, ε_p diagram. Starting from the value $\xi = \xi_c$, the increasing martensite fraction induced the increase of hardening rate and the radius of the limit surface tends to infinity.

The parameter $a = a(\xi)$ is a function of martensite volume fraction ξ and in view of Eq. (3.2), it can be expressed in term of plastic strain, so Eq. (4.3) is the Riccati equation. This equation may be integrated exactly for $a = \text{const.}$ Assuming $a^* = a(\xi^*)$, Eqs. (4.3) can be integrated along the loading path CF and the reverse loading path AC (Fig. 5). We may obtain for CF

$$(4.5) \qquad X(\varepsilon_p) = D \tan \left[2a^* C_1 D (\varepsilon_p + \varepsilon_{ap}) + \arctan \left(\frac{X_a}{D} - \frac{C}{6a^* D} \right) \right] + \frac{C}{6a^*},$$

and for FC

$$(4.6) \qquad X(\varepsilon_p) = D \tan \left[2a^* C_1 D (\varepsilon_p - \varepsilon_{ap}) + \arctan \left(-\frac{X_a}{D} + \frac{C}{6a^* D} \right) \right] - \frac{C}{6a^*},$$

where $D = \dfrac{\sqrt{18a^* - C^2}}{6a^*}$ and $a^* > \dfrac{C^2}{18}$.

Next, the relation between stress and plastic strain is specified, thus

$$(4.7) \qquad\qquad\qquad \sigma = R^* + X(\varepsilon_p) + a^* X(\varepsilon_p)^3.$$

The first step of the identification was to find the values of parameters C_1 and C in order to specify the steady state of the material, $R = R^*$, $\xi = \xi^*$, $a^* = a(\xi^*)$. The constants R^*, C and C_1 were determined, for different values of a^*, making use of common approximation of the hysteresis loops chosen from each load level (Fig. 1). The examples of approximation of the hysteresis loop and the cyclic
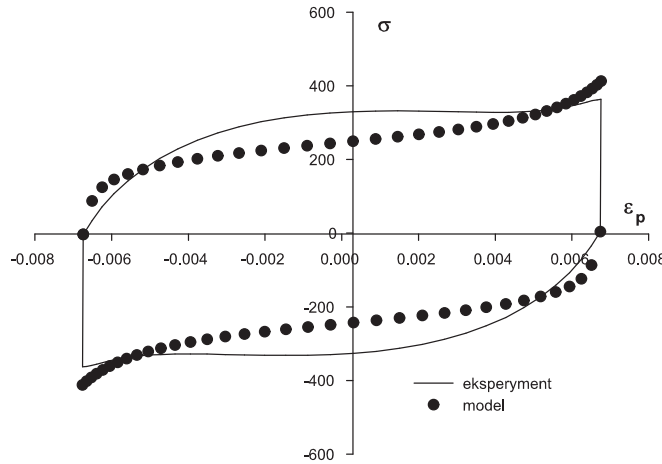

FIG. 7. The hysteresis loop at constant value of a $(a^* = 0.0001)$. The case $a(\xi) > a(\xi_c)$.
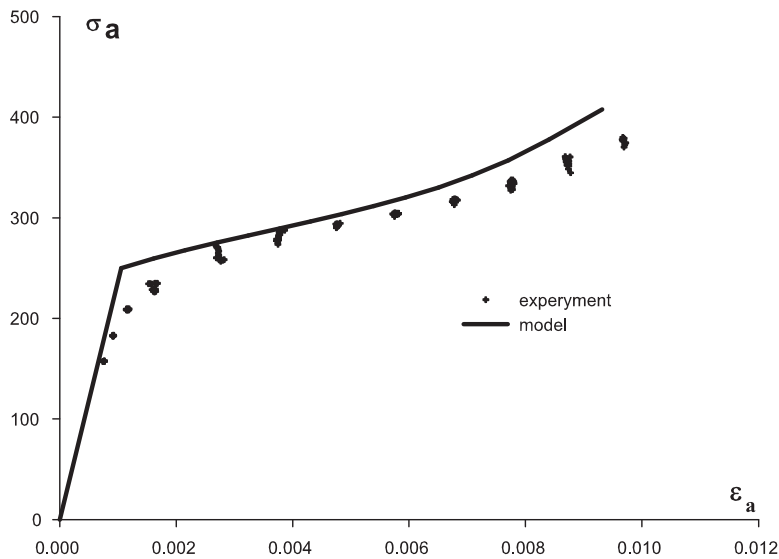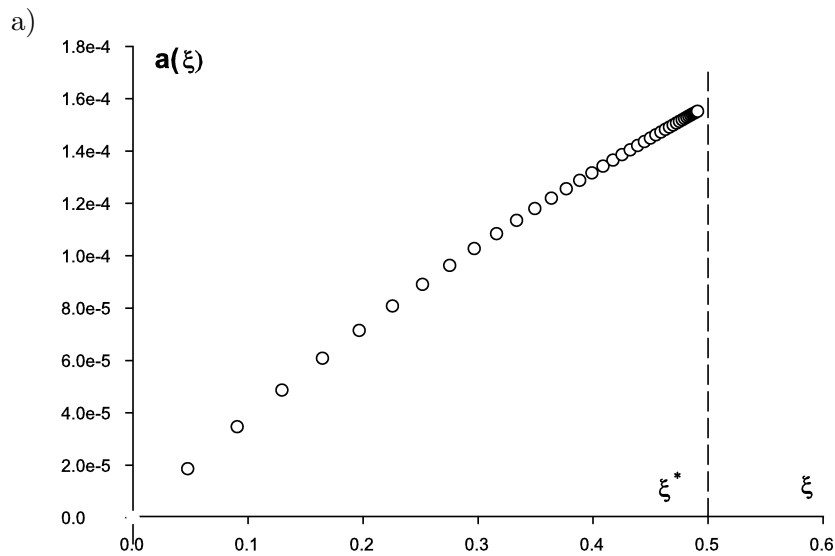
Fig. 8. Cyclic stress-strain curve at constant value of a $(a^* = 0.0001)$. The case $a(\xi) > a(\xi_c)$.

Next, we perform the simulation for two kinds of asymptotic convergence of the function $a(\xi)$, (Fig. 9). The values $C_1 = 48\,\text{GPa}$, $C = 0.027\,\text{MPa}^{-1}$ and $R^* = 150\,\text{MPa}$ are obtained as a result of identification of the experimental data for the steady state.
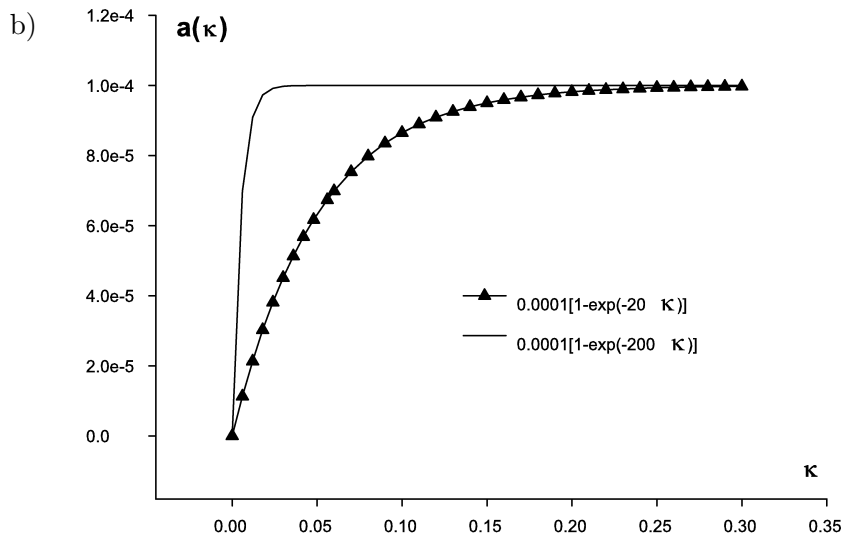
a)

[Fig. 9a]

b)

FIG. 9. The exemplary forms of the function a: a) $a = a(\xi)$, b) $a = a[\xi(\kappa)] = a(\kappa)$.

Results of the simulation for the constant strain amplitude ε_{ap} and two different kinds of the convergence of the function $a = a(\xi)$ are presented in Figs. 10 and 11.

However, the results of simulation for constant stress amplitude are presented in Fig. 12. The hysteresis loops for constant strain amplitude and constant stress amplitude stabilize very quickly, but we obtain the shift of the hysteresis loops for constant stress amplitude. This shift depends on the direction of first cycle (compression or tension).
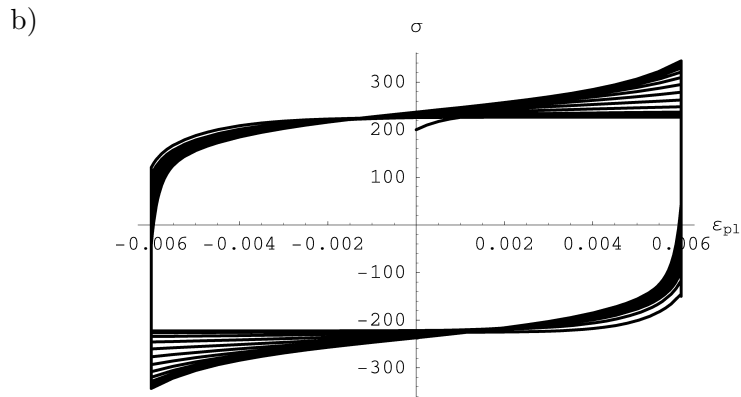
a)

[FIG. 10a]

b)
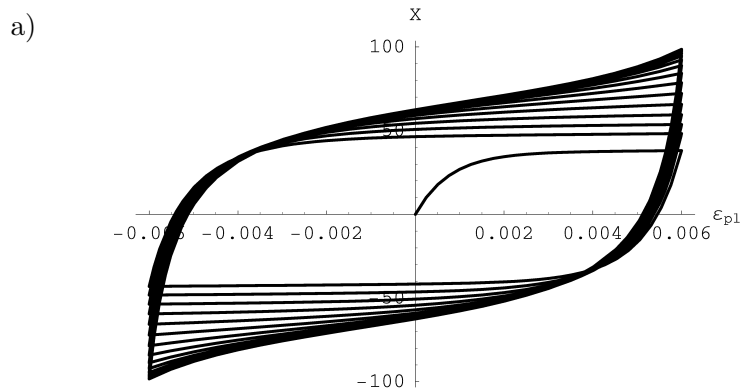
FIG. 10. The evolution of cyclic hysteresis loops for constant plastic strain amplitude
($\varepsilon_{ap} = 0.006$) and varying $a(\kappa) = 0.0001(1 - \exp(-20\kappa))$; a) plastic strain – back stress,
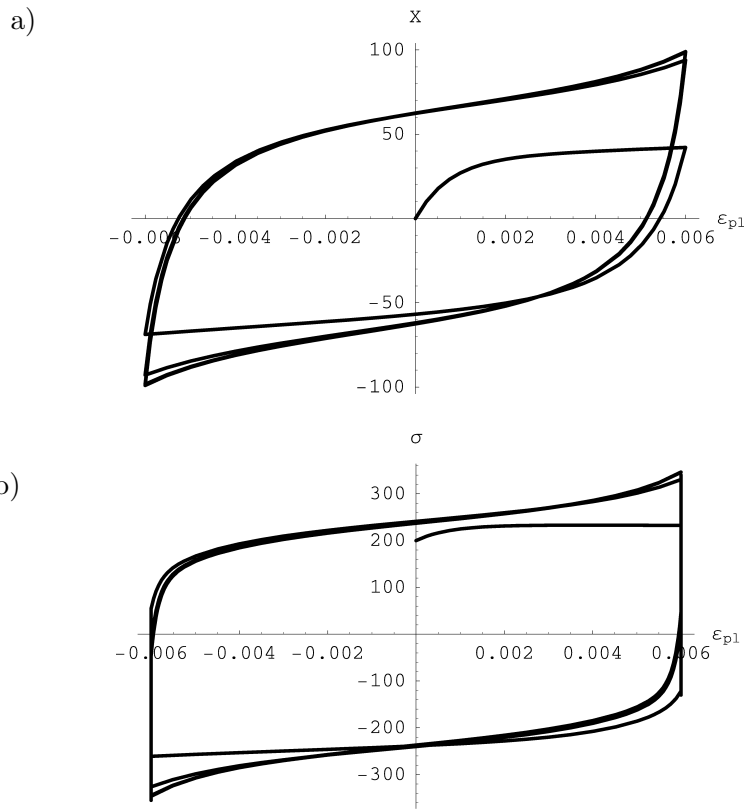b) plastic strain – stress.

a)

b)

FIG. 11. The evolution of cyclic hysteresis loops for constant plastic strain amplitude
($\varepsilon_{ap} = 0.006$) and varying $a(\kappa) = 0.0001(1 - \exp(-200\kappa))$: a) plastic strain – back stress,
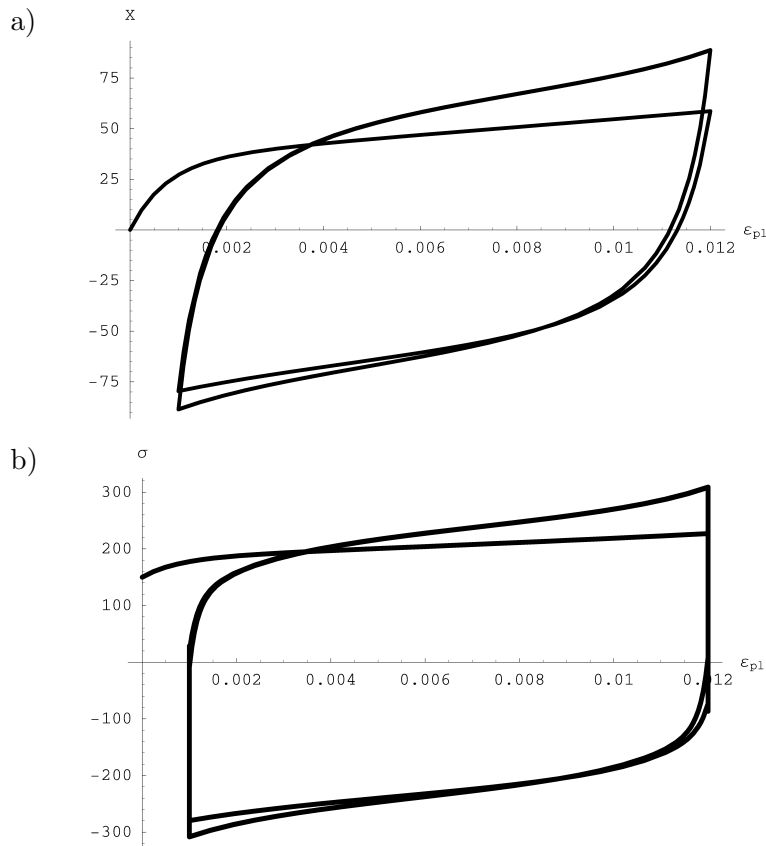b) plastic strain – stress.

a)

b)

Fig. 12. The evolution of cyclic hysteresis loops for constant stress amplitude
($\sigma_a = 300$ MPa): a) plastic strain – back stress, b) plastic strain – stress.

5. Conclusions

The paper presents an elasto-plastic model with possible appearance of the second phase – martensite in austenite. Constitutive equations were derived making use of irreversible thermodynamics with internal parameters. The modification of the yield surface allows the description of evolution of the hardening observed for such type of materials. The martensite volume fraction depends on the effective accumulated strain. This parameter may be determined in microscopic experiments. Such experiments may assist in selecting an adequate form of the evolution functions and offer information on the kinetics of phase transformation. However, quantitative description requires values resulting from the suitably designed macroscopic experiments. The function appearing in the phenomenological description is selected to fit the experimental data.

References

1. J. Kaleta, and G. Ziętek, *Representation of cyclic properties of austenitic steels with plasticity-induced martensitic transformation (PIMT)*, Fatigue and Fracture of Engineering Materials and Structures, **21**, 955–964, 1998.

2. A.A. Lebedev and V. V. Kosarchuk, *Influence of phase transformations on the mechanical properties of austenitic stainless steels*, Int. J. Plasticity, **16**, 749–767, 2000.

3. S. Ganesh Sundara Raman, and K.A. Padmanabhan, *Tensile deformation-induced martensitic transformation in AISI 304LN austenitic stainless steel*, J. Materials Science, Letters, **13**, 389–392, 1994.

4. M. Piwecki, *Strain-induced austenite transformation in 1H18N9 stainless steel under combined state of stress*, Arch. Metallurgy, **32**, 150–161, 1987.

5. H. Mughrabi and H-J. Christ, *Cyclic deformation and fatigue of selected ferritic and austenitic steels: specific aspects*, LSIJ International. **37**, 1145–1169, 1997.

6. K. I. Sugimoto, M. Kobayashi and S. I. Yasuki, *Cyclic deformation behavior of a transformation-induced plasticity-aided dual-phase steel*, Metall. and Mater.s Trans. A, **28A**, 2637–2644, 1997.

7. C. Garion and B. Skoczeń, *Modeling of strain-induced martensitic transformation for crygoenic applications*, J. Appl. Mech., **69**, 755–762, 2002.

8. P. Germain, Q.S. Nguyen and P. Suquet, *Continuum thermodynamics*, J. Appl. Mech., **50**, 1010—1020, 1983.

9. F.D. Fischer, *Transformation induced plasticity in triaxially loaded steel specimens subjected to a martensitic transformation*, Eur. J. A/Solids, **11**, 233–244, 1992.

10. M. Cherkaoui, M. Berveiller, and H. Sabar, *Micromechanical modeling of martensitic transformation induced plasticity (TRIP) in austenitic single crystals*, Int. J. Plasticity, **14**, 597–626, 1998.

11. Z. Mróz, *On the description of anisotropic workhardening*, J. Mech. Phys. Solids, **15**, 163–175, 1967.

12. Z. Mróz, and P. Rodzik, *On multisurface and integral description of anisotropic hardening evolution in metals*, Eur. J. Mech., A/Solids, **15**, 1–28, 1996.

Received February 14, 2006.